Journal of Geophysical Research, Solid Earth

Supporting Information for

Does Earthquake Stress Drop Increase with Depth in the Crust?

Abercrombie, R. E.[1*], D. T. Trugman[2], P. M. Shearer[3], X. Chen[4], J. Zhang[4], C. N. Pennington[4,5], J. L. Hardebeck[5], T. H. W. Goebel[6] and C. J. Ruhl[7]

1. Department of Earth and Environment, Boston University, Boston USA
2. Jackson School of Geosciences, University of Texas at Austin
3. Scripps Institution of Oceanography, University of California San Diego, La Jolla, CA
4. School of Geosciences, the University of Oklahoma, Norman, OK
5. USGS, Moffett Field, California
6. Center for Earthquake Research and Information, University of Memphis, 3890 Central Ave, Memphis, TN 38152
7. Department of Geosciences, The University of Tulsa, Tulsa, Oklahoma

Contents of this file

Figures S1 to S9: Supplementary Figures showing additional data sets, and results.
Tables S1 to S11: Velocity structures and sub-regions used in analysis.

Introduction

This supporting information contains Supplementary Figures showing additional examples of the data, and modeling with alternative inversion assumptions. The Supplementary Tables include the velocity models used in the analysis and plotted in Figure 2.

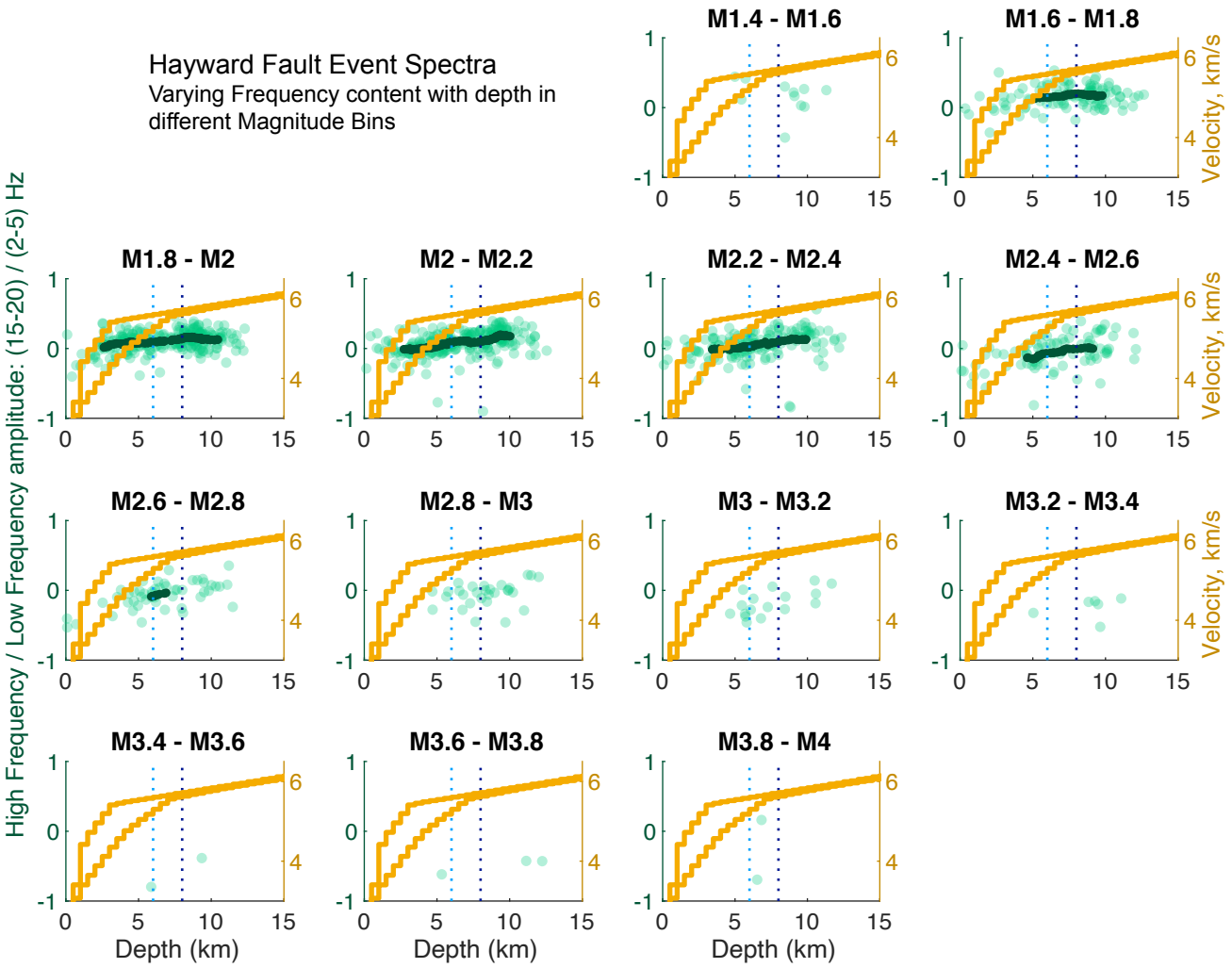

Figure S1. Ratio of high to low frequency spectral amplitude as a function of earthquake depth for earthquakes on the Hayward Fault (from Hardebeck & Aron, 2009); compare to Figure 2 in main paper. The event spectra are divided into 0.2 Mw unit bins (M=Mw) on the basis of their relative moments. Each plot shows the ratio of the mean high frequency (15-20 Hz) to mean low frequency (2-5.5 Hz) amplitudes of each event spectrum as a function of hypocentral depth (green circles). The running mean of 50 samples is also shown (dark green circles). The two vertical dashed lines indicate the selected cut-off depths used to determine the “deep” and “shallow” earthquakes. The pale orange lines are the 1D velocity structures (see Table 1). The spectra of deeper earthquakes have more high frequency energy, but this could represent increasing stress drop with depth, or decrease in attenuation with depth

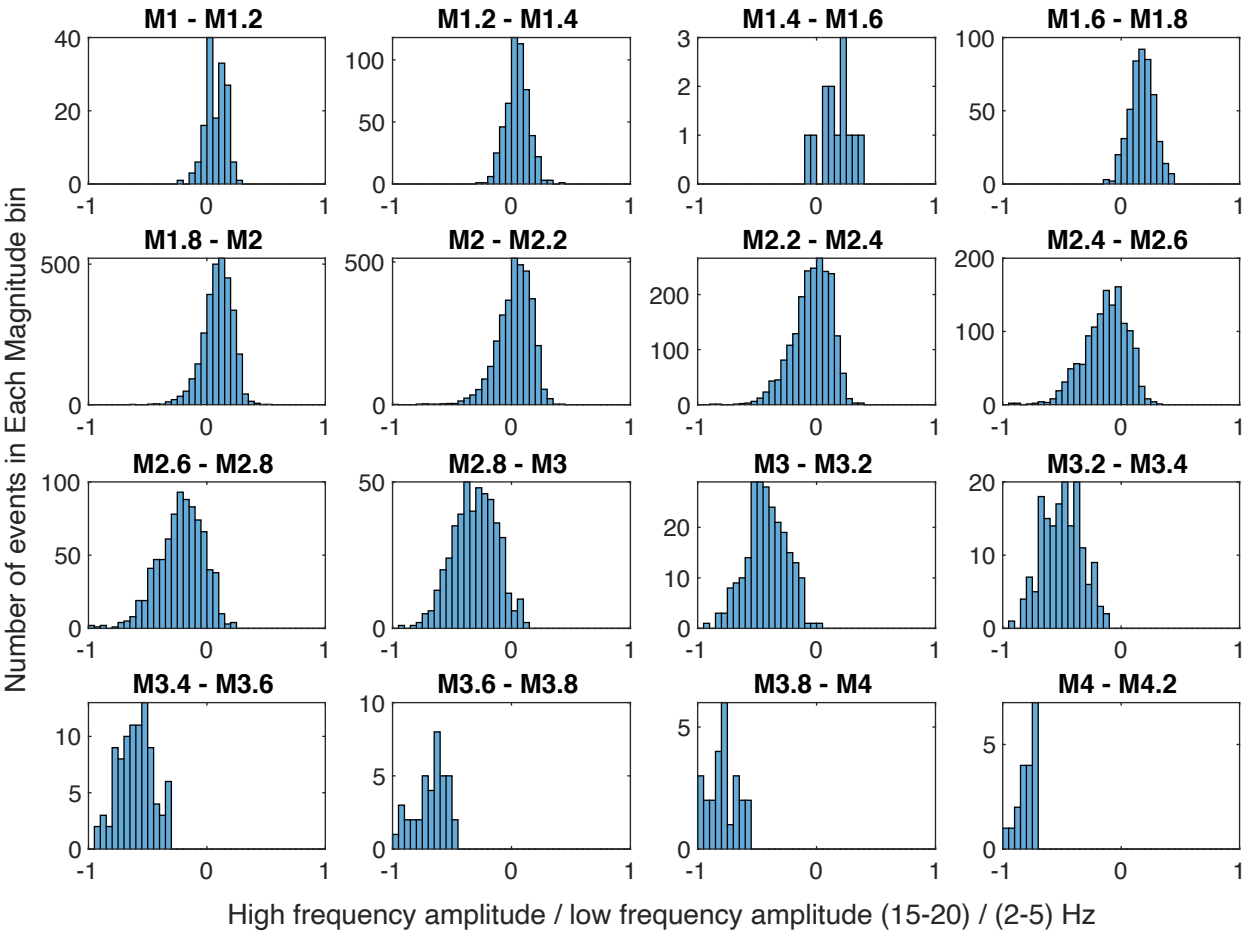

Figure S2. Histograms of numbers of Ridgecrest events plotted in corresponding panels of Figure 2 of main text.

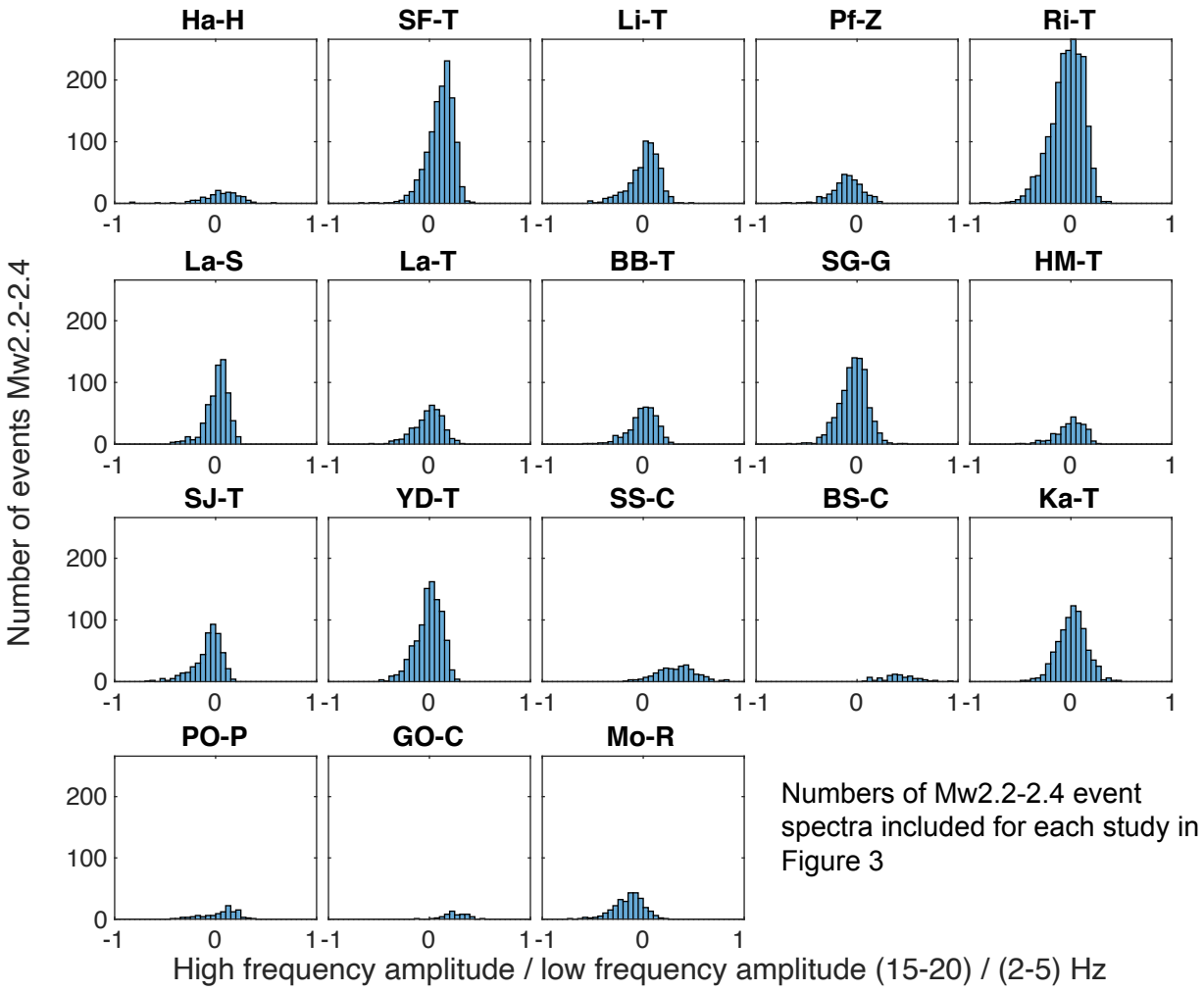

Figure S3. Histograms of numbers of events from each study plotted in corresponding panels of Figure 3 of main text.

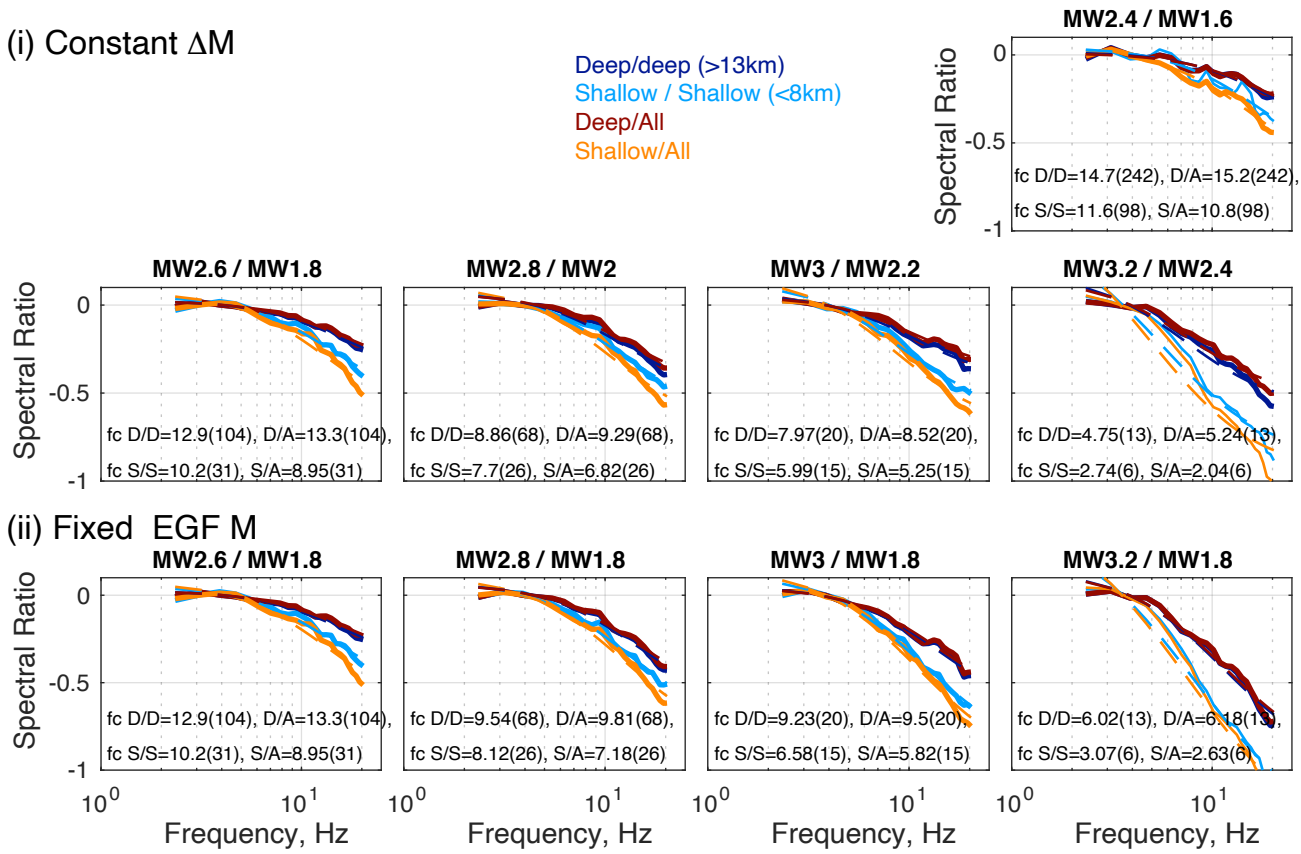

Figure S4a. Spectral ratios of stacked large to small San Gorgonio aftershocks, to investigate the effects of a depth dependent EGF correction (compare to Figure 6). Compare to the synthetic example in Figure 5. Each panel shows spectral ratios (solid lines) of the stacked large deep events to the stacked small deep events (dark blue), the large shallow events to the small shallow events (pale blue), the large deep events to all the small events (dark red) and the large shallow events to all the small events (orange). The title of each plot indicates the minimum Mw of the large and small events, both with a range of 0.2Mw. (i) is for a constant M difference between large and small earthquakes, and (ii) is for a constant-sized M for the small (EGF) earthquakes. The dashed lines are the fits of the Brune omega-squared spectral ratios to the average data ratios. The corner frequency of the best fitting ratio is given on each plot, with the number of larger events in the ratios in parentheses (D=deep, S=shallow, and A=all). Thinner lines indicate less than 10 large or small events were included in the mean ratios. The blue (depth-corrected) deep and shallow event spectral ratios are consistently closer together than the red ratios that assume no dependence of attenuation with depth (compare to Figure 5d,e).

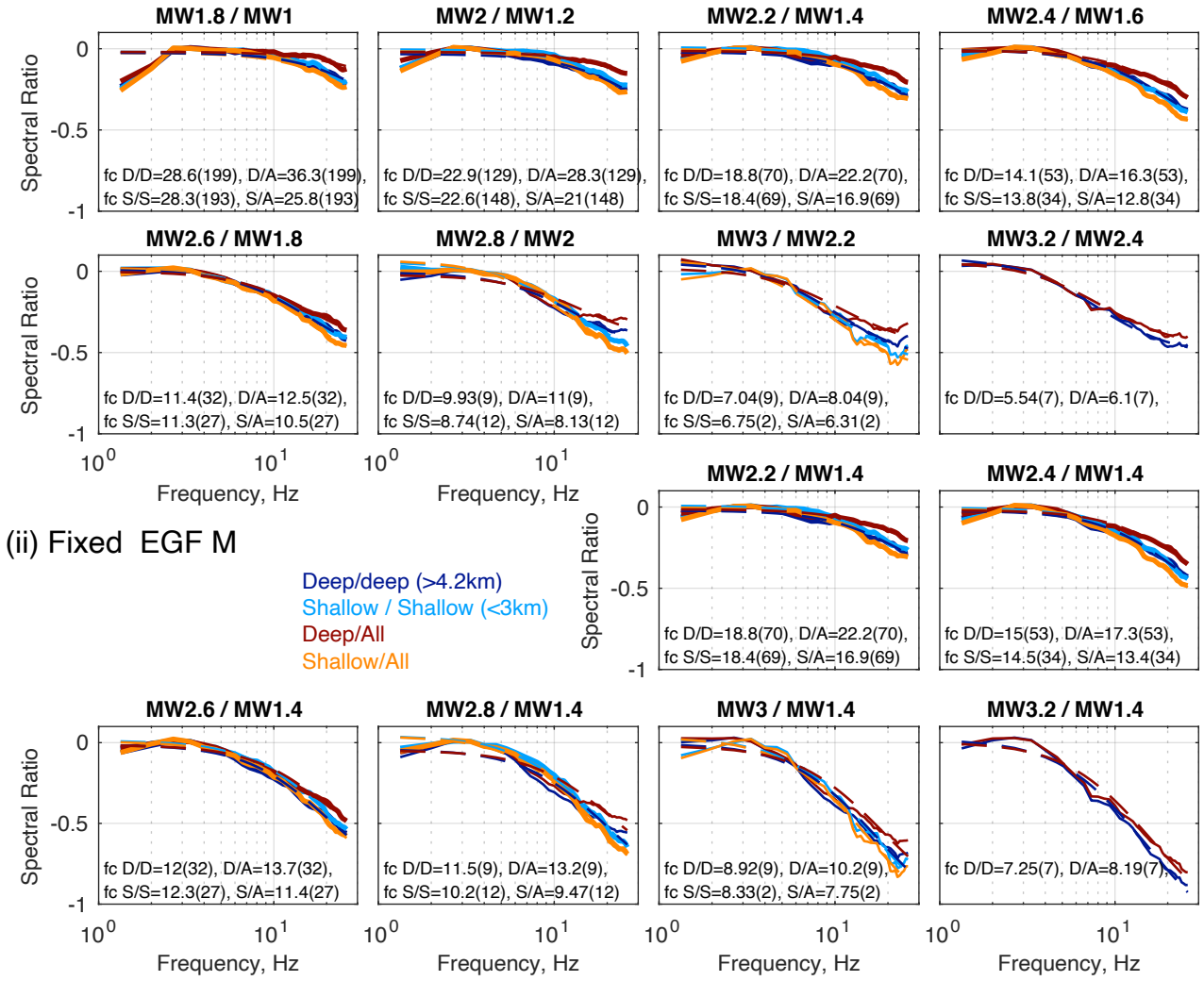

Figure S4b. Spectral ratios of stacked large to small Mogul, Nevada earthquakes: Compare to Figures 6 and S4a. Caption as for Figure S4a.

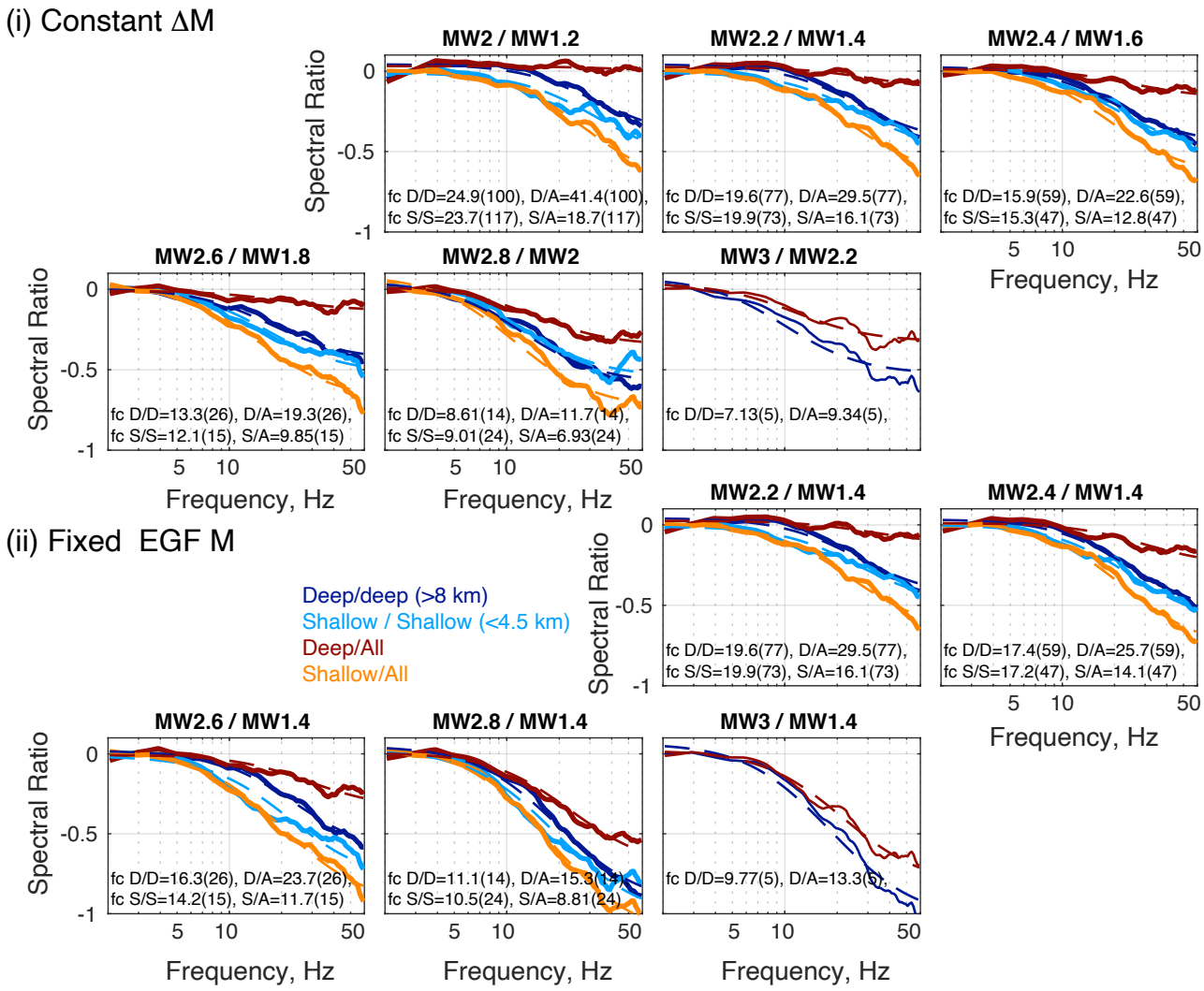

Figure S4c. Spectral ratios of stacked large to small Parkfield, California, earthquakes: Compare to Figures 6 and S4a. Caption as for Figure S4a.

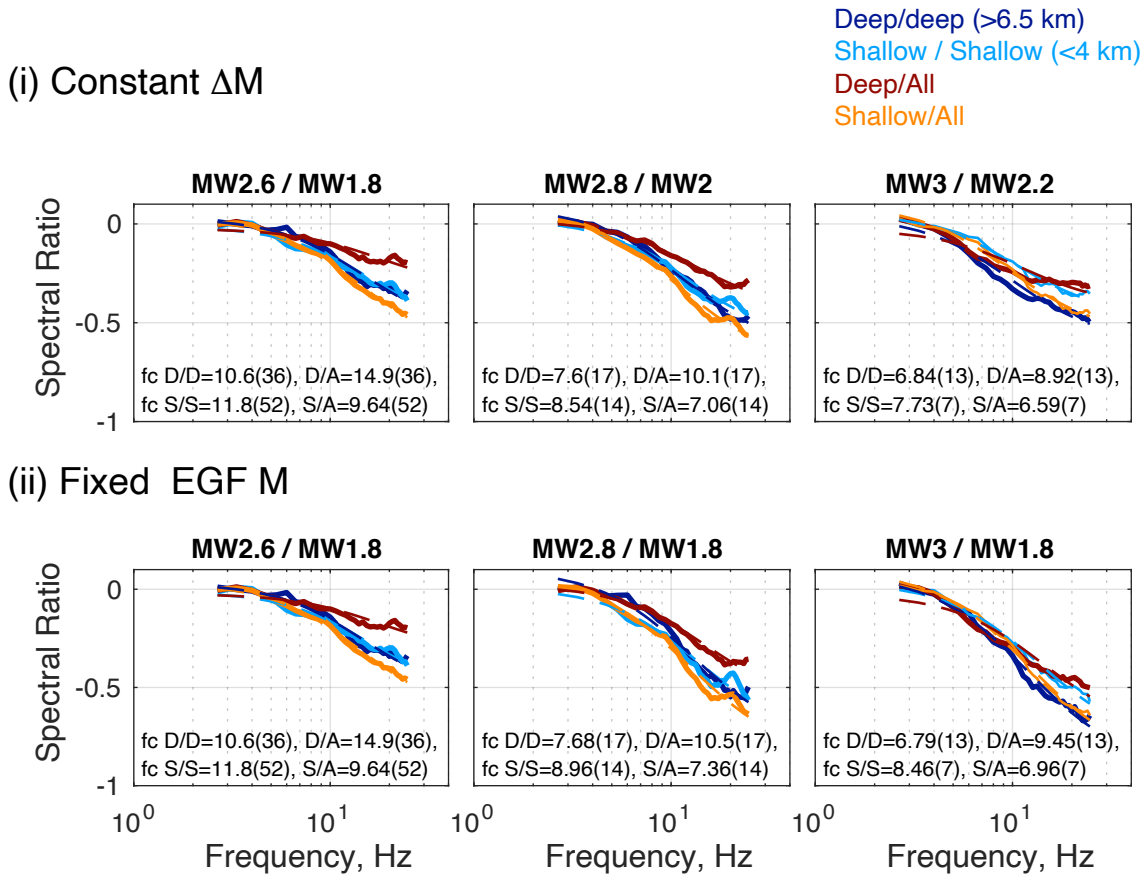

Figure S4d. Spectral ratios of stacked large to small Kansas, earthquakes: Compare to Figures 6 and S4a. Caption as for Figure S4a.

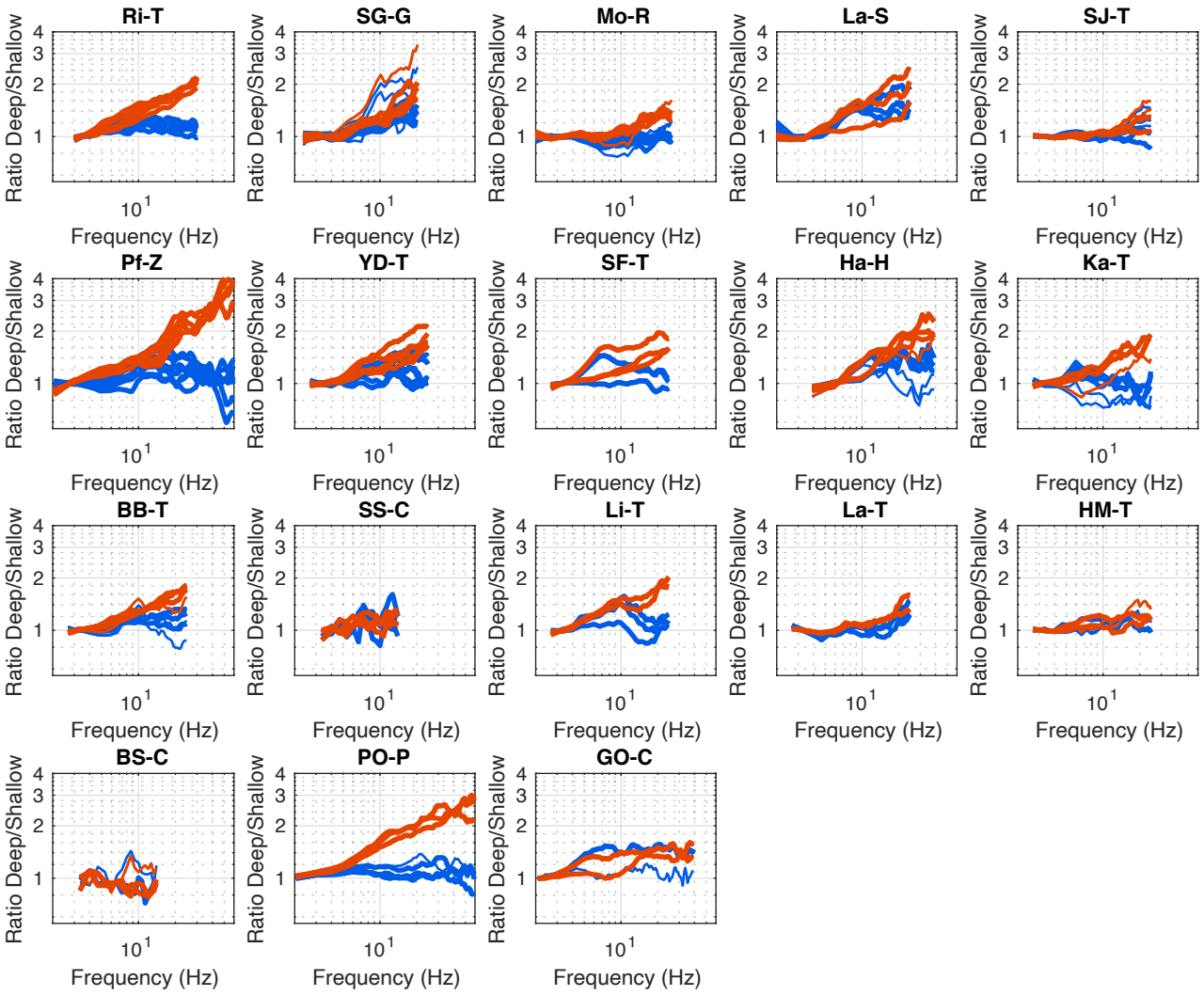

Figure S5. Depth differences in the event spectra: ratios of ratios – compare to Figure 5g,h,i. Same as Figure 7 in main text, but for all data sets considered.
Uncorrected for Depth (red symbols): The large deep and shallow events are divided by the same selection of small events, and so the difference between the deep and shallow ratios is simply the ratio of the mean deep large event spectra to the mean shallow.
Corrected for Depth (blue symbols). In this case, for each large M bin, the blue curve represents the ratio of the (mean large deep spectra divided by the small deep spectra) to the (mean large shallow spectra divided by the small shallow spectra). The similarity of the slope of the red curves in each region demonstrates that the difference in frequency content between shallow and deep events is independent of magnitude. The smaller slope of the blue curves shows that using the correct depth small EGF events can remove this depth-dependence to the frequency content, suggesting it is largely an attenuation effect.

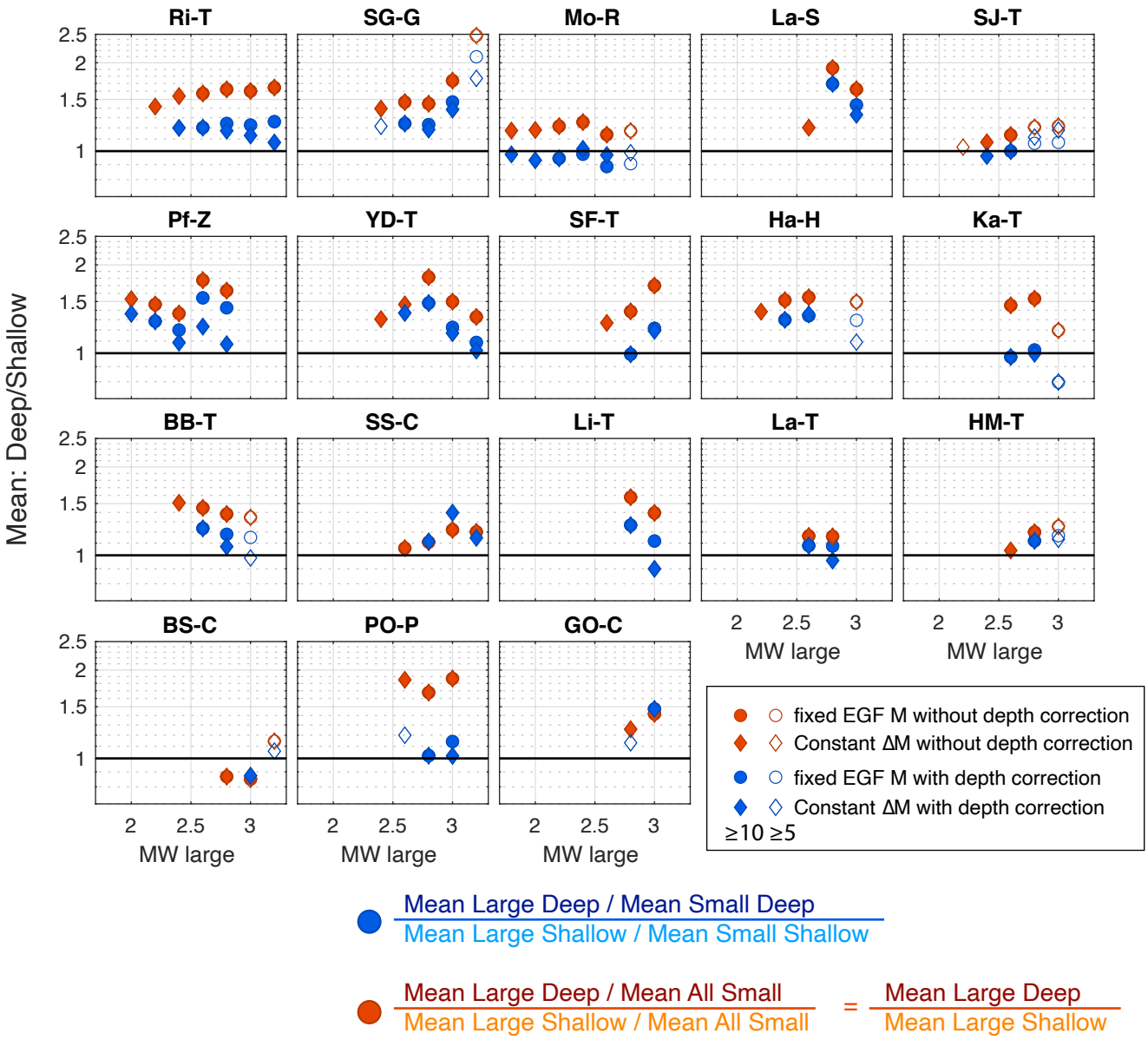

Figure S6. Comparison of mean amplitudes deep/shallow for each region – compare to Figure 3(g,h,i). Same as Figure 8 in main text, but for all data sets considered. The symbols indicate the mean values of the red and blue ratios shown in Figure 7, in the frequency range 2-20 Hz. Note that the depth correction is able to remove most, if not all, the difference between the deep and shallow spectra. The interpoint variation between diamonds and circles, and between different magnitudes is indicative of the uncertainties.

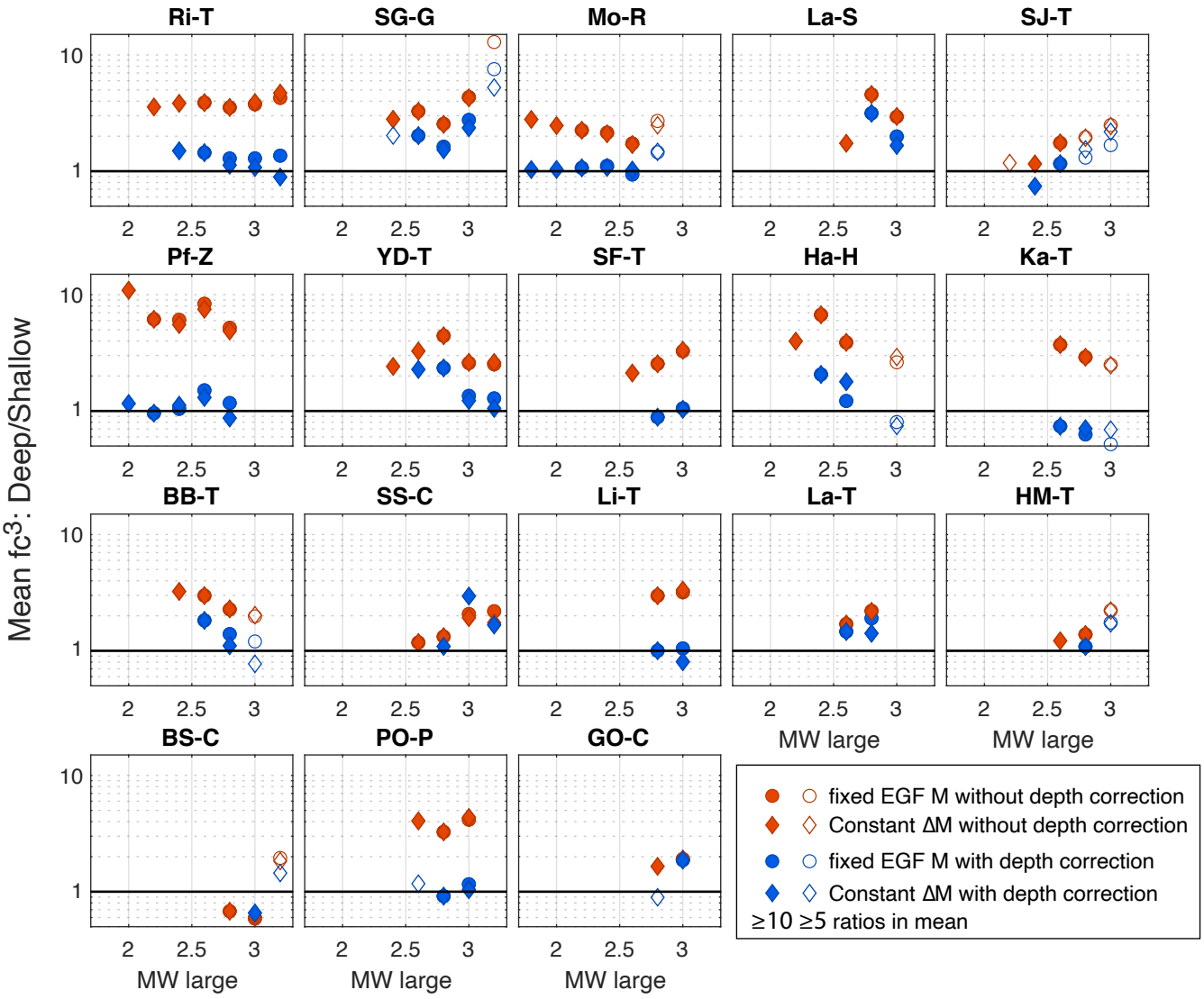

Figure S7. Spectral ratio modeling results with and without correction for depth-dependent attenuation. Same as Figure 9 in main text, but for all data sets considered. The ratios of the calculated stress drop (proportional to corner frequency cubed, fc^3) of the deep to the shallow earthquakes are shown for each data set, with (blue) and without (red) a correction for depth-dependent attenuation, plotted against the minimum magnitude of the large earthquakes. For example, the Ridgecrest plot shows the ratios of the cubed corner frequencies for the different model fits in Figure 9. Solid symbols represent ratios with at least 10 ratios, and open symbols those with at least 5; diamonds are for a constant different in magnitude between large and small, and circles are for a constant sized small event range. For most data sets, the depth corrections decrease the apparent difference in stress drop between the deep and small events, independent of the magnitude of the large or small events included.

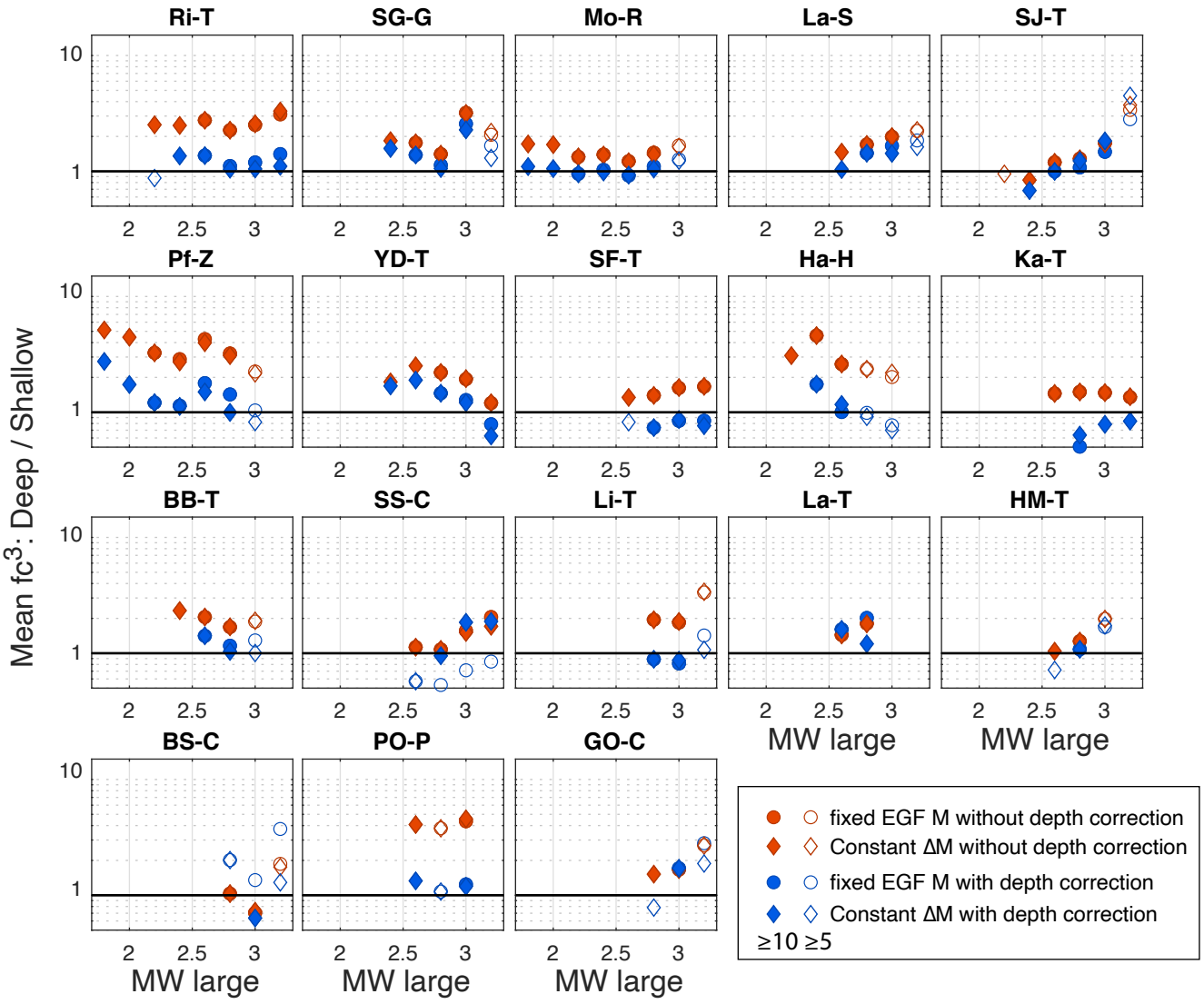

Figure S8a. Spectral ratio modeling results with and without correction for depth-dependent attenuation. Same as Figure S7 (and main text Figure 9) except that each data set is divided in half at the median depth and these halves as used as the deep and shallow depth populations. The trends observed are essentially unchanged from figure 9 and S8, implying that the results are not strongly dependent the depth ranges selected. Corner frequency cubed (fc^3) is proportional to stress drop.

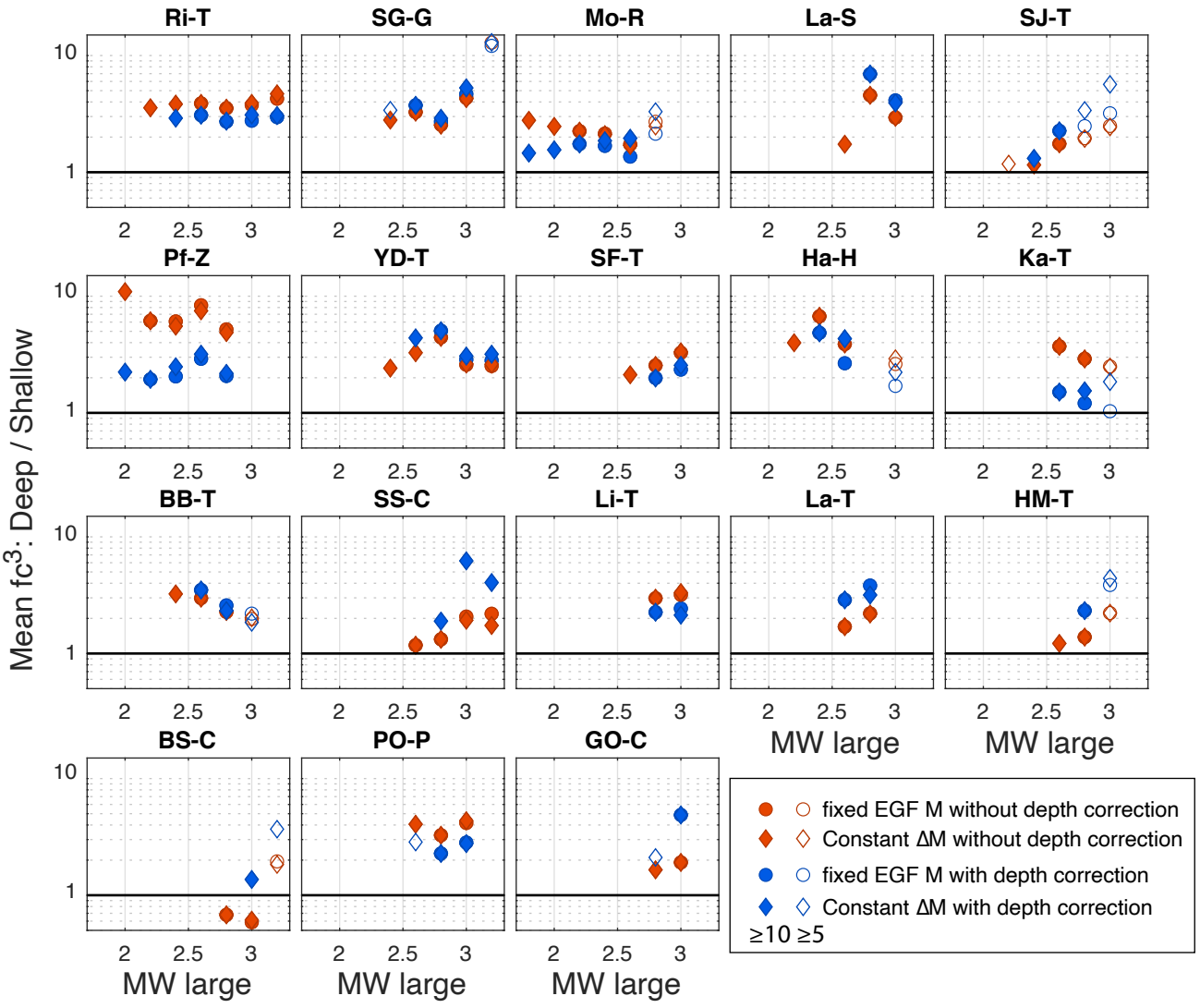

Figure S8b. Spectral ratio modeling results with and without correction for depth-dependent attenuation. Same as Figure S7 (and main text Figure 9), except stress drop for smaller earthquakes in deep depth range is fixed to a factor of 3 higher to simulate stress drop increasing with depth. Corner frequency cubed (fc^3) is proportional to stress drop.

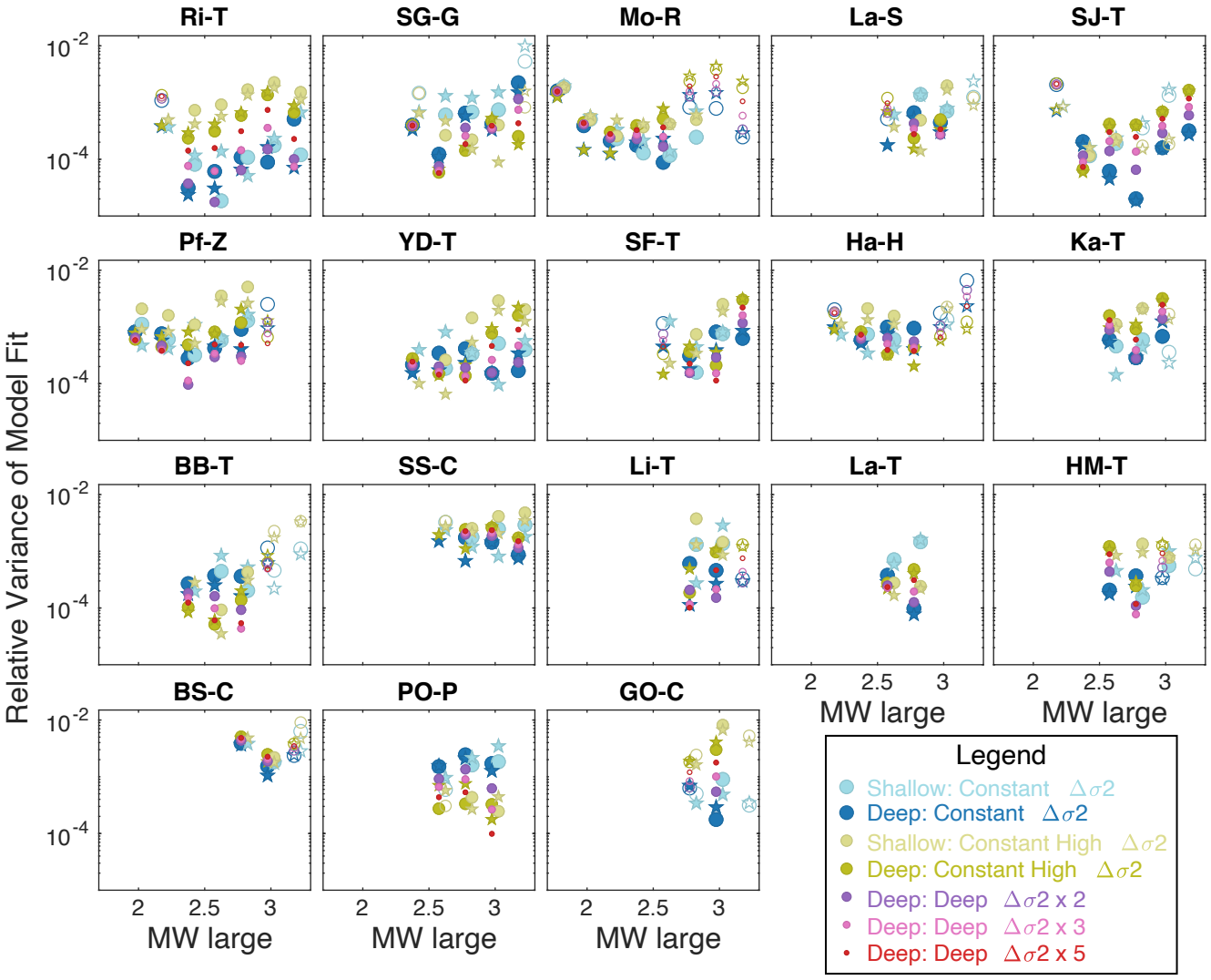

Figure S9. Variances of spectral ratio fits to the data, using different assumptions for the corner frequency of the denominator stack (fc_2). Circles are from constant ΔM, stars for fixed EGF M. Blue symbols are for the results shown in Figure 9, and green for an assumed higher stress drop for all the smaller events. Purple, pink and red are for deep, corrected ratios only, to show effects of an assumed depth increase in stress drop (e.g., Figure S8b, the shallow, and uncorrected-depth fits are the same as the blue symbols). Typically the blue or green have the lowest misfit variance, and the variance increases when fc_2 is allowed to increase with depth. For most data sets it is hard to distinguish between the high and low stress drop options for fc_2 (blue and green symbols), and there is no clear regional pattern. In Prague (OK) the higher assumed stress drop gives a better fit, but in Ridgecrest the lower assumed stress drop for the small events gives a better fit.

Table S1. Velocity Structure for Hayward Fault region (HA-H), manually digitized from Hardebeck and Aron (2009)

Depth to top of layer (km)	Vp east side (km/s)	Vp west side (km/s)
0.9877	3.6500	4.0500
3.0864	4.6000	5.2000
5.0617	5.2083	5.7167
7.2222	5.5000	5.8500
11.2346	6.0167	6.1000
17.4074	6.3167	6.2000
20.0000	6.4167	6.3333

Table S2. Velocity Structure for Bay Area Region (SF-T & Li-T), USGS San Francisco Bay Region 3D seismic velocity model (Aagaard *et al*., 2020)

Depth to top of layer (km)	Livermore Basin Vp (km/s)	Hayward+SAF east Vp (km/s)	Hayward+SAF west Vp (km/s)
0	1.8155	2.8371	1.8838
0.5	2.4215	3.0712	3.4070
1.0	2.9680	3.4047	4.4204
1.5	3.2856	3.6465	4.7226
2.0	3.6112	3.8860	4.9606
2.5	3.9303	4.1201	5.1937
3.0	4.2451	4.3511	5.4103
3.5	4.5099	4.5672	5.4531
4.0	4.7483	4.7647	5.4889
4.5	4.8932	4.9048	5.5182
5.0	5.0457	5.0474	5.5458
5.5	5.1876	5.1761	5.5757
6.0	5.3277	5.3022	5.6050
6.5	5.4643	5.4462	5.6342
7.0	5.5622	5.5585	5.6641
7.5	5.5968	5.6023	5.6983
8.0	5.6226	5.6307	5.7221
8.5	5.6609	5.6738	5.7546
9.0	5.6872	5.7031	5.7819
9.5	5.7276	5.7458	5.8142
10.0	5.7560	5.7736	5.8409
10.5	5.7975	5.8155	5.8735
11.0	5.8256	5.8406	5.8962
11.5	5.8707	5.8780	5.9329
12.0	5.8976	5.9032	5.9548
12.5	5.9417	5.9385	5.9925
13.0	5.9658	5.9622	6.0142
13.5	6.10	5.9975	6.0533
14.0	6.0249	6.0207	6.0761
14.5	6.06	6.0574	6.1162
15.0	6.0843	6.0852	6.1390
15.5	6.1185	6.1327	6.1770
16.0	6.1424	6.1626	6.2025
16.5	6.1785	6.2075	6.2389
17.0	6.2033	6.2389	6.2680

17.5	6.2428	6.2893	6.3051
18.0	6.2711	6.3263	6.3342
18.5	6.3479	6.3853	6.3778
19.0	6.4069	6.4071	6.4018

Table S3. Velocity Structure for Parkfield region (Pf-Z), Thurber *et al.* (2006)

Depth to top of layer (km)	Vp SW (km/s)	Depth to top of layer (km)	Vp NE (km/s)
0	2.75	0	3.00
0.50	3.00	0.50	3.50
1.00	3.50	0.75	3.75
1.50	4.00	1.00	4.00
2.75	4.50	1.50	4.50
4.00	5.00	2.00	5.00
9.00	5.50	3.75	5.50
14.00	6.00	5.50	6.00
15.50	6.25	12.00	6.50
17.00	6.50	20.00	6.50
20.00	6.50		

Table S4. Velocity Structure for Mogul, Nevada (Mo-R), Ruhl *et al.* (2016)

Depth to top of layer (km)	Vp (km/s)
0	3.5
1	4.5
2	5.5
4	6.0
7	6.4
18	6.8

Table S5. Velocity Structure for Ridgecrest, California (Ri-T), Lomax (2020)

Depth to top of layer (km)	Vp (km/s)
-5	4.78
0	5.37
3	5.79
6	6.13
9	6.18
12	6.30
15	6.41
20	6.51
32	7.80

Table S6. Velocity Structure for Southern California regions (Landers: LA-T, Big Bear: BB-T, Hector Mine: HM-T, San Jacinto Trifurcation Zone: SJ-T, and Yuha Desert: YD-T), SCEC Community Model (Shaw *et al*., 2015; Small *et al.,* 2017)

Depth to top of layer (km)	La-S Vp (km/s)	La-T Vp (km/s)	BB-T Vp (km/s)	HM-T Vp (km/s)	SJ-T Vp (km/s)	YD-T Vp (km/s)	SG-G Vp (km/s)
-1	3.9825	0	3.2615	0	0	0	0
0	4.7214	4.7860	4.7173	4.8082	5.1053	3.4022	4.7097
1	4.9717	5.0854	4.9734	4.9990	5.2782	5.1330	4.9402
2	5.2275	5.3822	5.2265	5.1923	5.4524	5.2812	5.1367
3	5.4643	5.6669	5.4737	5.3818	5.6301	5.3964	5.3352
4	5.5889	5.7500	5.6035	5.5788	5.7437	5.4791	5.5274
5	5.6926	5.8276	5.7429	5.7729	5.8680	5.5670	5.7291
6	5.8193	5.9013	5.8682	5.9657	5.9701	5.6554	5.9094
7	5.8604	5.9325	5.9100	5.9903	6.7200	5.6860	5.9625
8	5.8836	5.9551	5.9233	6.9900	6.0272	5.7319	6.3800
9	5.9225	5.9877	5.9507	6.0306	6.0387	5.7584	6.0461
10	5.9642	6.0181	5.9760	6.0473	6.0489	5.7862	6.0856
11	6.90	6.0609	6.0191	6.0934	6.0777	5.8765	6.1115
12	6.0562	6.1000	6.0595	6.1412	6.1063	5.9711	6.1356
13	6.0973	6.1425	6.1020	6.1893	6.1322	6.0772	6.1585
14	6.1381	6.1818	6.1391	6.2357	6.1558	6.1944	6.1825
15	6.1513	6.2111	6.1751	6.2580	6.1779	6.2125	6.2019
16	6.2060	6.2714	6.2466	6.3298	6.2595	6.4138	6.2277
17	6.3669	6.3499	6.2626	6.4052	6.2978	6.4468	6.2678
18	6.3554	6.3750	6.3172	6.4317	6.3322	6.4664	6.3210
19	6.4077	6.4076	6.3403	6.4465	6.3740	6.4747	6.3580
20	6.4312	6.4321	6.3862	6.4762	6.4120	6.4946	6.4045
21	6.4579	6.4577	6.4256	6.4982	6.4506	6.5073	6.4489
22	6.5054	6.4863	6.4574	6.5223	6.4970	6.5200	6.4845
23	6.5120	6.5140	6.4792	6.5410	6.5090	6.5358	6.5061
24	6.5453	6.5384	6.5088	6.5586	6.5236	6.5446	6.5351
25	6.5671	6.5588	6.5277	6.5690	6.6268	6.5637	6.5519
26	6.5900	6.5787	6.5568	6.5880	6.9159	6.6570	6.5764
27	6.6112	6.5985	6.5804	6.7602	7.1815	6.7014	6.5980
28	6.6263	6.6236	6.6029	7.5633	7.3205	7.3118	6.6153
29	6.6568	6.7803	6.6214	7.7788	7.5418	7.6264	6.6320
30	6.6668	7.0292	6.6357	7.7788	7.5418	7.8032	6.6496

Table S7. Velocity Structure for Salton Sea (SS-C) and Bawley Seismic Zone (BS-C) regions, from SCEC Community Model (Shaw *et al*., 2015; Small *et al.,* 2017), and local model from Chen and Shearer (2011)

Depth to top of layer (km)	BS-C CVM Vp (km/s)	SS-C CVM Vp (km/s)	Depth to top of layer (km)	Vp (km/s), Chen & Shearer
-1	0	0	0	4.1929
0	0	0	0.2	4.2938
1	2.0103	2.5327	0.4	4.3947
2	2.9211	3.9740	0.6	4.4956
3	3.8320	4.8400	0.8	4.5964
4	4.6175	4.9427	1.0	4.6973

5	5.3435	5.3233
6	5.3922	5.6512
7	5.5904	5.8212
8	5.8227	5.9890
9	6.0592	6.1654
10	6.3084	6.3391
11	6.4611	6.4063
12	6.5793	6.4715
13	6.6924	6.5497
14	6.8221	6.6162
15	6.9433	6.6910
16	6.6681	6.5138
17	6.5473	6.4869
18	6.5482	6.4850
19	6.5439	6.4970
20	6.5477	6.5106
21	6.5532	6.5240
22	6.5617	6.5353
23	7.1248	7.7290
24	7.8113	7.8097
25	7.8113	7.8097
26	7.8113	7.8097
27	7.8113	7.8097
28	7.8113	7.8097
29	7.8113	7.8097
30	7.8113	7.8097

1.2	4.7982
1.4	4.8991
1.6	4.9999
1.8	5.1800
2.0	5.2017
2.0	5.2017
2.2	5.2674
2.4	5.3330
2.6	5.3987
2.8	5.4644
3.0	5.5300
3.2	5.5957
3.4	5.6614
3.6	5.7270
3.8	5.7927
4.0	5.8584
4.0	5.8584
4.2	5.8842
4.4	5.9101
4.6	5.9360
4.8	5.9619
5.0	5.9877
5.2	6.0136
5.4	6.0395
5.6	6.0653
5.8	6.0912
6.0	6.1171
6.2	6.1429
6.4	6.1688
6.6	6.1947
6.8	6.2205
7.0	6.2464
7.2	6.2577
7.4	6.2690
7.6	6.2802
7.8	6.2915
8.0	6.3028
8.2	6.3141
8.4	6.3254
8.6	6.3367
8.8	6.3479
9.0	6.3592
9.2	6.3705

9.4	6.3818
9.6	6.3931
9.8	6.4044
10.0	6.4156
10.2	6.4239
10.4	6.4321
10.6	6.4404
10.8	6.4486
11.0	6.4569
11.2	6.4651
11.4	6.4734
11.6	6.4816
11.8	6.4899
12.0	6.4981
12.2	6.5064
12.4	6.5146
12.6	6.5229
12.8	6.5311
13.0	6.5394
13.2	6.5476
13.4	6.5559
13.6	6.5641
13.8	6.5724
14.0	6.5806
14.2	6.5935
14.4	6.6064
14.6	6.6192
14.8	6.6321
15.0	6.6449
15.2	6.6578
15.4	6.6707
15.6	6.6835
15.8	6.6964
16.0	6.7092
16.2	6.7221
16.4	6.7350
16.6	6.7478
16.8	6.7607
17.0	6.7736
17.2	6.7864
17.4	6.7993
17.6	6.8121
17.8	6.8250

18.0	6.8379
18.2	6.8501
18.4	6.8623
18.6	6.8745
18.8	6.8866
19.0	6.8988
19.2	6.9110
19.4	6.9232
19.6	6.9354
19.8	6.9476
20.0	6.9598

Table S8. Velocity Structure for Southern Kansas (Ka-T), Rubinstein *et al.* (2018).

Depth to top of layer (km)	Vp (km/s)
0	2.600
0.25	3.850
1.75	5.450
2.50	5.950
8.00	6.200
21.00	6.300
42.00	7.800

Table S9. Velocity Structure for Guthrie Oklahoma (GO-C), Chen (2016).

Depth to top of layer (km)	Vp (km/s)
-1.50	2.67
1.30	5.67
4.10	6.15
6.90	5.93
9.80	6.21
12.60	6.26
15.40	6.17
18.20	6.20
21.00	6.24
23.80	6.43
26.70	6.62
29.50	6.79
32.30	6.97
35.10	7.16
37.90	7.34
40.70	7.45
43.60	7.56
46.40	7.75
49.20	7.96
52.00	8.14

Table S10. Velocity Structure for Prague, Oklahoma (PO-P), digitized from Toth *et al.* (2012)

Depth to top of layer (km)	Vp (km/s)
-0.2365	2.5948
-0.1260	2.6038
0.1143	2.7915
0.2611	2.9961
0.3979	3.1078
0.7379	3.3100
0.8895	3.4377
1.0410	3.5029
1.1554	3.7570
1.1967	3.9537
1.2510	4.1456
1.3408	4.5872
1.4098	4.7125
1.4518	4.8972
1.4746	5.0912
1.5234	5.3071
1.6415	5.5730
1.6835	5.6993
1.7719	5.8013
1.9496	5.7924
2.0770	5.8347
2.1884	5.8758
2.3174	5.9134
2.4632	5.9537
2.6196	6.0010
2.7603	6.0487
2.8936	6.0922
3.0417	6.1083
3.1588	6.1029
3.3109	6.1244
3.4417	6.1208
3.6053	6.1440
3.7489	6.1440
3.8604	6.1440
3.9841	6.1387
4.0970	6.1530
4.2178	6.1619
4.3349	6.1565
4.4890	6.1780
4.6238	6.1744
4.7709	6.1959
4.9118	6.1923
5.0416	6.2066
5.1774	6.2102
5.3204	6.2281
5.4319	6.2066
5.7798	6.2334
5.9733	6.2495
6.1061	6.2459
6.2717	6.2692
6.4204	6.2638

6.5438	6.2781
6.6627	6.2817
6.7854	6.3049
7.1191	6.3109
7.2721	6.3175
7.4437	6.3369
7.6407	6.3547
7.8247	6.3765
7.9641	6.3765
8.0743	6.3765
8.2426	6.3982
8.4381	6.4152
8.6122	6.4331
8.7966	6.4467
8.9831	6.4599
9.1496	6.4837
9.3101	6.5034
9.4686	6.5255
9.6067	6.5195
9.7233	6.5374
9.8577	6.5570
9.9722	6.5642

Table S11. Coordinates (Longitude and Latitude, in decimal degrees) of Polygons used to select sub-regions for analysis:

Table S11a: Bay Area Hayward Fault SF-T

-122.4223	38.0010
-122.7698	37.9803
-122.5213	37.4795
-122.2859	36.9189
-121.7442	36.8982
-121.4304	37.0636
-121.7610	37.5300
-122.1384	37.8034
-122.3009	38.0010

Table S11b: Bay Area Livermore Basin Li-T

-121.8700	37.5828
-121.6142	37.7391
-121.5886	37.8432
-121.7447	38.0893
-121.9007	38.1982
-122.1974	38.1343
-122.2691	38.0657
-122.2358	37.9852
-122.0747	37.7675
-121.9442	37.6420

Table S11c: Salton Sea, Geothermal Region SS-C

-115.5644	33.1516

-115.6611 33.1132
-115.6867 33.1790
-115.6288 33.2065
-115.5595 33.2424
-115.4857 33.2538
-115.4541 33.2348
-115.4464 33.2008
-115.4977 33.1677

Table S11d: Salton Sea, Brawley Seismic Zone BS-C

-115.5838 33.1314
-115.6463 33.0997
-115.5442 32.8778
-115.5004 32.8487
-115.4691 32.8664
-115.5223 33.0439